World Electric Vehicle Journal

MDPI

Article

Power Flow and Voltage Control Strategies in Hybrid AC/DC Microgrids for EV Charging and Renewable Integration

Zaid H. Ali [1,2,*] and David Raisz [1]

[1] Department of Electrical Power Engineering, Budapest University of Technology and Economics, Egry J. u. 18, 1111 Budapest, Hungary
[2] Renewable Energy Research Unit, Hawija Technical Institute, Northern Technical University, Mosul 41002, Iraq
* Correspondence: zaidali@edu.bme.hu

Abstract: This study outlines the creation and lab verification of a low-voltage direct current (LVDC) back-to-back (B2B) converter intended as a versatile connection point for low-voltage users. The converter configuration features dual inverters that regulate the power distribution to AC loads and grid connections through a shared DC circuit. This arrangement enables the integration of various DC generation sources, such as photovoltaic systems, as well as DC consumers, like electric vehicle chargers, supported by DC/DC converters. Significant advancements include sensorless current estimation for grid-forming inverters, which removes the necessity for conventional current sensors by employing mathematical models and established system parameters. The experimental findings validate the system's effectiveness in grid-connected and isolated microgrid modes, demonstrating its ability to sustain energy quality and system stability under different conditions. Our results highlight the considerable potential of integrating grid-forming functionalities in inverters to improve microgrid operations.

Keywords: LVDC; droop control; electric vehicle chargers; bidirectional power flow

Academic Editors: Jianguo Zhu, Yu Wang and Weiwei Geng

Received: 12 January 2025
Revised: 7 February 2025
Accepted: 9 February 2025
Published: 14 February 2025

Citation: Ali, Z.H.; Raisz, D. Power Flow and Voltage Control Strategies in Hybrid AC/DC Microgrids for EV Charging and Renewable Integration. *World Electr. Veh. J.* **2025**, *16*, 104. https://doi.org/10.3390/wevj16020104

1. Introduction

There has been a significant increase in the installation of distributed generators in electricity distribution systems, particularly from renewable sources like solar and wind. The rise of electric vehicles (EVs) is further complicating demand by introducing irregular charging patterns, leading to increased variability and uncertainty in load profiles. Frequent connections and disconnections of loads also contribute to the challenges in maintaining stability and reliability in distribution networks.

A study developed a coordinated power management control strategy for a low-voltage microgrid (MG) integrating solar photovoltaic (PV) and storage. The strategy guarantees an equitable power distribution among DG sources and facilitates mode transitions. Grid-supporting, grid-forming VSIs are utilized with modified droop and virtual output impedance control strategies. The control method regulates voltage and frequency levels in accordance with (Australian Standard) AS4777. MATLAB-Simulink 2023b is used for the simulations and analyses [1]. The performance of an adaptive recursive digital filter control is demonstrated in a solar PV-powered electric vehicle battery (EVB) grid-connected system. The system supplies active power to the grid and enhances the power quality at the PCC. The EVB stores and releases energy dependent on the peak demand. Maximum Power Point Tracking (MPPT) and battery charging/discharging both utilize bidirectional converters. The technique of recursive filtering ensures that there is no phase delay between the

fundamental and load currents. The experimental results validate the unity power factor operation, elimination of harmonics, and IEEE-519 compliance. Under various conditions, the system exhibits both a steady state and a dynamic response. The voltage source inverter (VSC) functions as an active power filter and reactive power compensator. The control technique is validated by means of the test results [2]. It evaluates existing controllers in terms of their advantages and limitations. Local power distribution systems, renewable energy resources, and energy storage techniques are investigated. Consideration is given to the dependability and stability of power transmission using voltage source inverters.

Using various controllers and soft computing algorithms, the paper introduces the concept of microgrids in both islanding and grid-connected modes. It concisely summarizes controllers and their applications in microgrid systems [3]. The rise in electric vehicles poses a charging challenge. A solar-powered charging station with battery storage and grid support is the most plausible solution. The PID and voltage control keep the station's DC bus voltage constant. The design is validated in MATLAB/Simulink using multiple operation modes and EV specifications. This scalable solution is suitable for large power ratings in workplaces and parking lots [4]. The literature proposes a coordinated control technique for hybrid AC/DC microgrids that is efficient. Battery Active Droop Control (BADC) and Battery Demand Droop Control (BDDC) control systems are modified with correction terms. The strategy ensures stable operation of the storage system and subgrids and appropriate power interaction and subgrid support during power fluctuations. The simulations validate the method's efficacy [5]. Researchers introduced a novel DC grid for a charging station. PV/storage and DC/DC converters furnish the utility with renewable energy for EV charging. It is appropriate for locations that lack access to AC utility infrastructure, such as highways. A storage system is incorporated into the system to mitigate PV power variations. The phase shift full bridge (PSFB) converter enhances the voltage levels and system dependability. Solar irradiance, temperature, and EV power demand profiles are used to evaluate the model. The proposed system is confirmed by MATLAB/Simulink simulations [6].

The focus of the discussion is on how to use electric railway power systems (ERPSs) and electric vehicles (EVs) to reduce carbon emissions. It proposes a sophisticated DC catenary system that interconnects the ERPS with renewable energy sources, storage systems, and DC fast-charging stations. For power processing, the system employs dedicated DC/DC power converters and includes a storage system for backup and continuous power supply. It introduces optimal power control and a power management system (PMS). The effectiveness of the proposed system is validated using the actual data from a high-speed rail line and simulation results [7]. A study proposed a control system for an autonomous and grid-connected solar PV/battery-based microgrid. In grid-connected mode, the control strategy enhances power quality and ensures unity power factor operation. It comprises power management, reactive power compensation, power factor correction, and harmonics mitigation. The system remains stable in autonomous mode and can accommodate grid failure or generation and load demand disparities. In off-grid mode, the PV array and battery supply the demand with high-quality voltages. The simulation and laboratory experiments validate the efficacy of the system [8].

The increased use of electric vehicles has increased the demand for EV charging stations. DC grid-based charging that employs renewable energy sources (RESs) and energy storage units (ESUs) is more efficient. Strategies for energy management and control are essential for optimal operation. This review examines the various architectures, control strategies, and power converter topologies used in EV charging stations that are connected to renewable energy sources. Microgrid-based architectures, energy management systems, and charging converter controllers are compared. Various charging station models, controls,

and connectors are discussed. A strategy for energy management based on experimentation maximizes RES consumption. The paper discusses the challenges, opportunities, and selection criteria for charging stations [9]. The proposed unified control scheme for a dual-stage grid-connected PV system allows for a seamless transition between MPPT and droop phases. A DC/DC converter governs the voltage of the DC bus. A resonant controller eliminates second-order harmonics for the reliable operation of PV sources. The controller of the DC/AC converter implements the mode transition. A self-tuning algorithm modifies the droop coefficient in response to inadequate solar irradiance. Experiments and simulations are conducted on PV/battery microgrid testbeds to demonstrate the proposed design [10,11]. A paper presents a model of a Wind/PV/Battery microgrid that is grid-connected and consists of a photovoltaic generator, a wind turbine, and battery storage. It implements maximum power point monitoring algorithms for optimized power extraction and an energy management system for efficient energy distribution. The simulation results demonstrate that the proposed control and management strategies are effective [12].

A reliable and robust battery current controller is suggested to resolve transient load issues and guarantee correct charging/discharging cycles, thereby extending battery life. During load variations, the controller minimizes overshoot, rise time, and settling time while sustaining the DC-link voltage. A modified PI-based feedback control technique is presented for current control of the battery energy storage system. The proposed system is verified using the OPAL-RT Lab (NIT Kurukshetra, India) platform and simulated in MATLAB [13].

Another paper describes a three-phase microgrid with multiple photovoltaic arrays and a central battery energy storage (BES) system. The PV arrays and BES are coupled to the point of common coupling (PCC) using VSCs. To regulate the VSCs connected to the PV arrays, a mode of current/power sharing is implemented. In grid-interfaced mode, the BES-VSC is controlled to maintain constant power sharing with the grid, and in standalone mode, it is controlled to maintain voltage and frequency at the PCC. The frequency, phase, and fundamental active weights of the grid and load voltages are estimated using a frequency-locked loop based on a second-order sequence filter (SOSF-FLL) [14].

A study examines a DC microgrid that combines wind and solar technologies to provide reliable power in remote areas. It utilizes a Permanent Magnet Synchronous Generator (PMSG) for wind power and solar panels for DC generation. A battery storage system and MPPT-based converters optimize energy utilization. The study reviews microgrid management systems and proposes energy management strategies. A MATLAB/Simulink model demonstrates the power flow within the microgrid [15]. A paper simulates a grid-connected PV and EV charging system that supports grid-to-vehicle (G2V) and vehicle-to-grid (V2G) power transmission. Various converters are utilized, including a boost converter for PV power, a bidirectional buck–boost converter for EV charging, and a VSC for grid integration. The PV power extraction utilizes MPPT, and controllers regulate power flow and voltage. The system maximizes PV energy output, guarantees uninterrupted EV charging, enhances utility performance, and employs EVs as energy storage. Extensive MATLAB/Simulink simulations validate the system's efficacy under various conditions [16]. The focus of the discussion is on the control design of a two-stage electric vehicle charger, with particular attention to the first-stage AC/DC converter. A reduced-order plant-integrated proportional integrating (PIPI) controller is proposed for enhanced grid support. Traditionally, a proportional resonant (PR) regulator is used to monitor grid current; however, the complexity of this third-order system increases its difficulty. In response, a first-order PIPI regulator is devised, which provides the same capabilities as a PR regulator while reducing the complexity. The proposed method is implemented in the inner current control loop of

the AC/DC converter, resulting in an enhanced dynamic response and simplified controller design compared to the conventional PR regulator [17].

An article describes a distributed solar PV and battery energy storage DC microgrid comprising interconnected nanogrids for power sharing. A nanogrid with excess power can share it with a nanogrid experiencing load shedding due to the microgrid architecture. The upper controller ensures that only excess power is shared, prohibiting the nanogrid from entering load-shedding mode. The lower- and upper-level controllers use a dc bus signalling strategy to monitor and modulate local bus voltage and control power sharing. When surplus power is available, the simulation results validate the efficacy of the proposed microgrid structure, which facilitates power sharing to prevent load shifting among nanogrids [18].

An article presents a centralized energy management system (CEMS) for the efficient and dependable administration of a DC microgrid. The CEMS optimizes PV and battery energy storage, performs optimal load shedding, and regulates DC bus voltage. The simulation results demonstrate the efficiency and dependability of the proposed method for optimizing energy utilization and enhancing microgrid performance [19]. A paper describes a PV-based charging station equipped with a battery energy storage system. The test results validate the enhanced power quality operation of the EV charging station under dynamic conditions, including intermittent PV insolation and various modes of battery energy storage. Also examined in depth is the system's response during battery charging and discharging [20].

A hybrid equalization (HE) framework for lithium-ion batteries (LIBs) was examined, which merges both active and passive voltage equalization methods to effectively address cell imbalance. Different configurations, involving a combination of active and passive equalization at both the individual cell and pack levels, were assessed, with a focus on evaluating response times and SOC levels. The results indicated that hybrid equalization markedly improves both equalization speed and efficiency compared to using only one strategy, offering a balanced approach to maintain optimal SOC [21].

Control schemes for a low-voltage back-to-back converter were examined, focusing on maintaining the DC bus voltage and power flow through a PI-controlled closed-loop system. Grid voltage synchronization was achieved using the SRF-PLL, and the system's effectiveness was validated through simulations in MATLAB/SIMULINK and laboratory experiments. The proposed methods ensured balanced power control and minimized oscillations in power exchange [22].

The growing popularity of EVs is driving an urgent need for enhanced charging infrastructure, underscoring the importance of establishing robust and widespread networks. To ensure efficient operation, EV charging stations must adopt innovative strategies to manage peak demand, provide convenient charging options, and enhance grid stability. Integrating energy storage systems (ESS), such as batteries and supercapacitors, addresses these challenges by balancing load variations and enabling the integration of renewable energy sources. Recently, HESS, which combines multiple ESS technologies, has been more effective than individual systems by leveraging their complementary characteristics, such as the rapid response time of lithium-ion batteries and the energy capacity of redox flow batteries. These systems guarantee enhanced performance, decreased reliance on the grid, and an extended lifespan for batteries used in EV charging stations [23,24].

To tackle these issues, this research suggests a new hybrid AC/DC microgrid architecture incorporating advanced control strategies for managing energy flow, improving grid stability, and enabling efficient integration of renewable energy sources. The proposed LVDC B2B system facilitates smooth interaction between the AC and DC networks through a common DC-link, presenting a flexible solution for incorporating PV systems, EVs, and

ESSs. The system guarantees reliable operation in grid-connected and islanded modes by utilizing bidirectional power flow capabilities, providing a solid framework for varied load and generation conditions.

- In laboratory settings, practical limitations like restricted access to analog current sensors make the testing and validating of grid-forming inverter systems more challenging. To overcome this, the proposed system uses mathematical models and established system parameters to indirectly calculate the load current ($I_{L,dq}$) from measurable quantities, including capacitor voltages and inverter currents. This method removes the necessity for additional sensors at the load or capacitor, simplifying the hardware configuration while ensuring precision and making it suitable for laboratory environments with limited resources.
- The goals of this research are outlined as follows: Developed a hybrid AC/DC microgrid design that integrates PV systems, ESSs, and EV chargers, enabled by an innovative bidirectional LVDC B2B converter. This configuration not only boosts energy distribution effectiveness but also provides isolation from low-voltage public networks, enhancing safety and reliability throughout the grid.
- Created and executed a hybrid control approach that combines grid-forming capabilities with droop-based voltage and frequency regulation to ensure stable operation in both grid-connected and islanded conditions. This advancement is further reinforced by the incorporation of sensorless current estimation techniques that simplify hardware requirements and enhance the precision of current measurements.
- Confirmed the proposed system's performance and efficiency through extensive simulations using MATLAB/Simulink and practical experimental setups. The empirical findings illustrate the system's capacity to facilitate smooth transitions between different operational modes, sustain DC bus voltage stability, and effectively balance power under diverse operating conditions.

2. System Structure

The microgrid system now under examination is shown in Figure 1. It consists of a grid inverter, Home Load Inverter (HLI), PV panels, EV, and storage battery charger. The bidirectional buck–boost DC/DC converter maintains a constant DC-link voltage, which will secure a steady power supply to the home load in the absence of the grid. Between the AC and DC sides, the grid-connected converter permits power exchange. The DC/DC boost converter integrates the P&O MPPT capabilities to maximize power extraction from the PV panels. Depending on the system's operating parameters, a bidirectional buck–boost converter is used to charge and discharge the storage and EV batteries.

Multimode controller combinations are necessary because the PV-based grid system uses an EV and storage unit charging system. An inner fast current loop regulates the *dq*-axis current, and an outside slower voltage loop controls the DC-link voltage (i_d and i_q). Two PI controllers are needed to manage the electricity's active and reactive flow into the grid, since the *d*- and *q*-axis values are coupled. The PI controller regulates the DC-link voltage by reducing the difference between the reference and measured voltage values, which also serve as a reference for the d-axis current (i_d*) [16]. The line current vector must be aligned with the line voltage vector; as a result, the *q*-axis current reference is set to zero (i_q* = 0). The *dq*-axis current expression is as follows:

$$L\frac{d_{id}}{dt} = v_d + k_p v_d{}' - k_i i_d + \omega L i_q \quad (1)$$

$$L\frac{d_{iq}}{dt} = v_q + k_p v_q{}' - k_i i_q + \omega L i_d \quad (2)$$

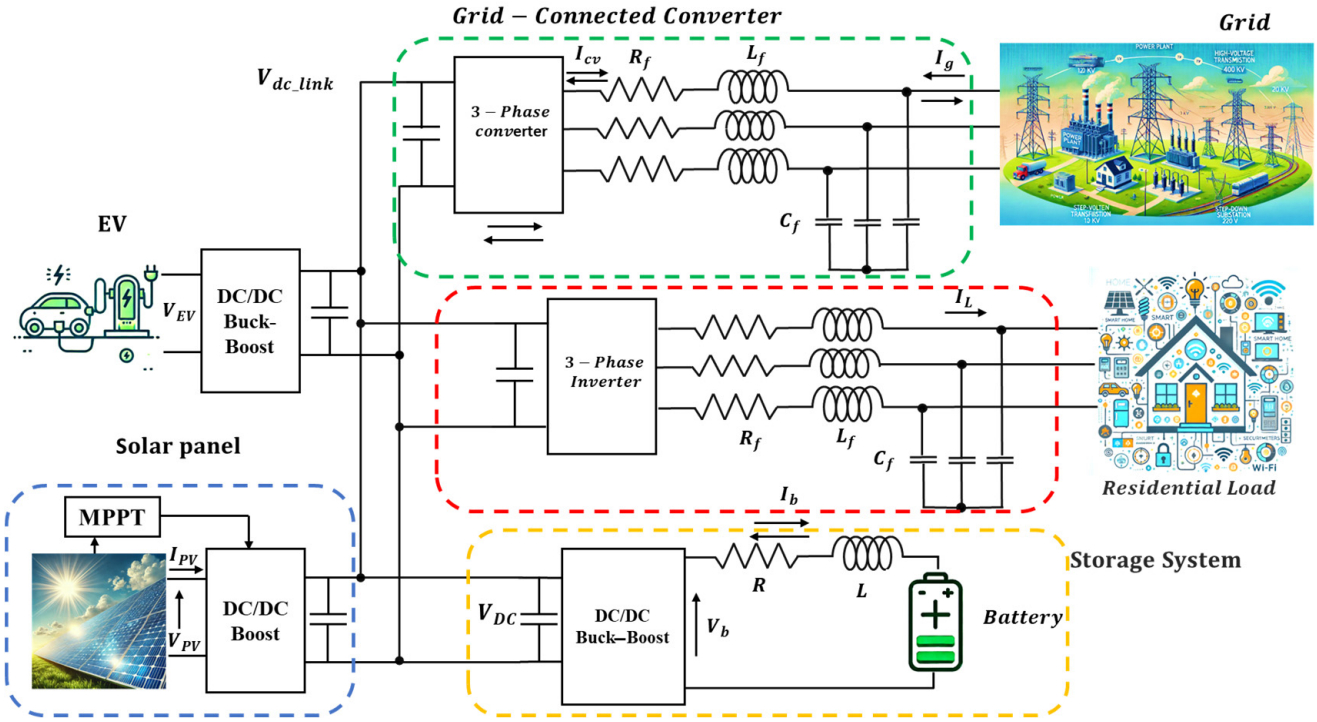

Figure 1. Grid-connected microgrid general architecture.

Under the assumption of negligible inverter losses, the active and reactive power equations can be described using the line inductance (L) and the angular frequency of the grid (w).

$$P = \frac{3}{2}(v_d i_d + v_q i_q) \tag{3}$$

$$Q = \frac{3}{2}(v_d i_q - v_q i_d) \tag{4}$$

Because the voltage vector is aligned with the d-axis since $i_q^* = 0$, we obtain:

$$P = \frac{3}{2}(v_d i_d) \tag{5}$$

$$Q = 0 \tag{6}$$

A control system that regulates power distribution according to the solar PV availability and SOC is depicted in Figure 2: Modes of power flow. Mode one maintains the battery charge while diverting excess PV power to the grid when the SOC is higher than 95%. When the PV output is low (less than 0.2), mode two takes over, using battery power to assist the grid (vehicle-to-grid, or V2G if EVs are involved). In order to ensure energy availability during periods of lower solar generation, mode three is activated when both the SOC and PV are below 95%. This enables the grid to charge the batteries. This control logic ensures effective energy management over a range of solar production and storage levels.

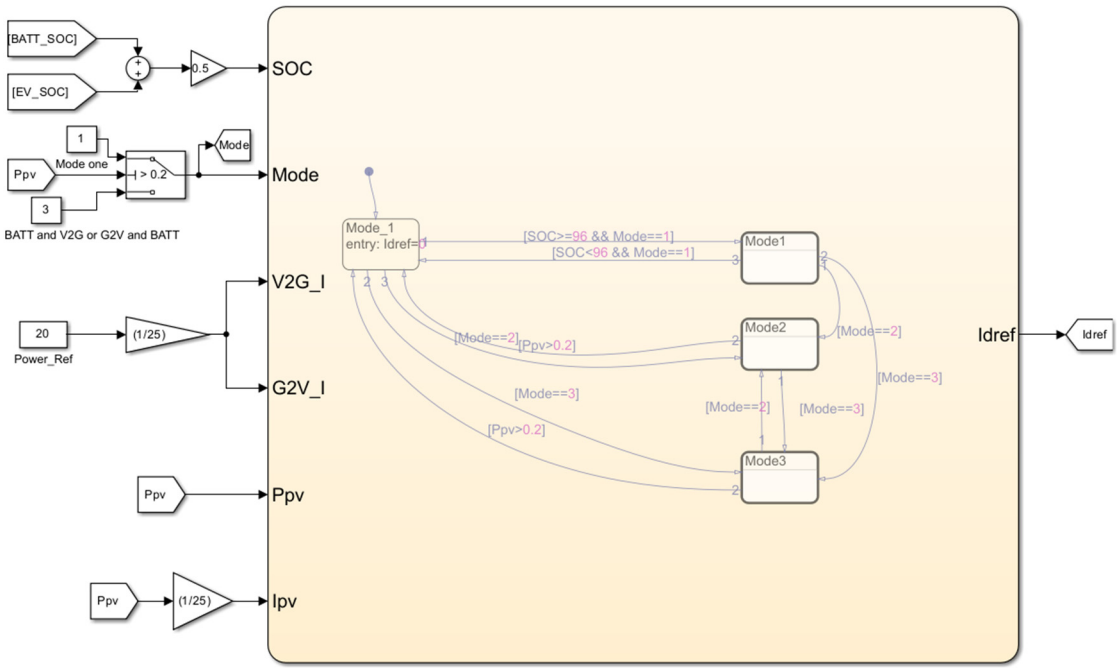

Figure 2. Modes of power flow.

3. Modes of Power Flow Control

In mode one, the solar PV system controls the power supply based on the state of charge (SOC), EV, and storage batteries. If the SOC of both batteries is greater than 95%, the solar PV energy is directed toward supplying the grid and HLI. If the SOC declines below 95%, solar PV power is used to charge the EV and storage batteries and power the HLI.

In the mode of selection, the SOC is utilized as a criterion. If the SOC is at least 95%, the control system receives a reference current value, I_{dref}, to supply energy to the grid. However, if the SOC is below 95%, the Idref is set to zero, indicating no power will be provided to the grid. This decision is based on the recharge requirements of the batteries and the solar PV system's surplus power availability.

In mode two, the energy flow is configured to supply the grid from the EV and storage batteries. Setting the current reference value I_{dref} to one indicates that power will be supplied to the grid. The EV and storage batteries are utilized as energy sources to contribute to the grid's energy demands and power the HLI.

In mode three, the power flow is reversed, and the grid charges the EV and the storage batteries. This is done by setting the current reference value I_{dref} to (-1), which indicates that power will be drawn from the grid. In this mode, the energy source for recharging the EV and storage batteries is the grid and powering the HLI.

4. Bidirectional DC/DC Buck–Boost Converter of Batteries

The bidirectional DC/DC buck–boost converter plays a critical role in linking the storage units to the DC-link system. This converter facilitates power transfer in both directions, allowing energy to be supplied to and drawn from the storage units as needed.

Since renewable energy sources can be unreliable, as a backup during outages, storage units become crucial. These storage units can capture excess energy produced by renewable sources during high output and release it when the energy demand surpasses what renewable generation can provide. This ensures a consistent power supply and reduces dependence on the grid during fluctuating renewable energy production periods.

The mathematical model of the storage system considers two key variables: the voltage at the system's endpoint and the state of charge of the storage units. These elements are vital for efficiently managing and regulating the storage facilities.

Figure 3 depicts the construction of the storage device converter, consisting of a bidirectional DC/DC buck–boost converter and a battery. The operation of the converter is determined by the duty cycle (D) of the switches *S1* and *S2*. Based on the configurations of these switches, the converter's operation can be divided into two modes:

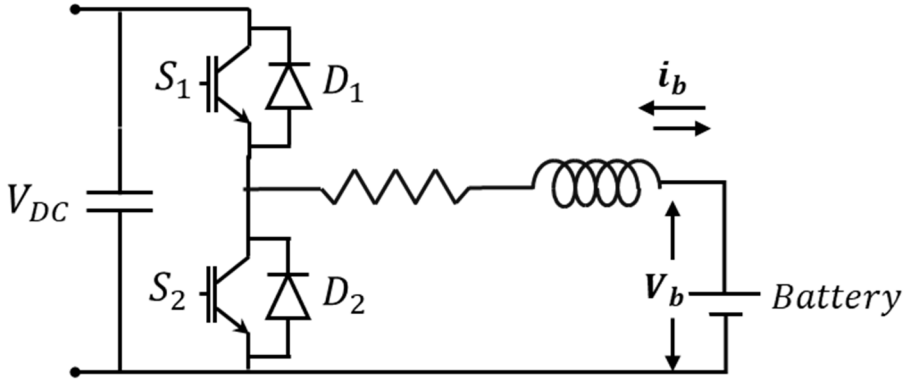

Figure 3. EV and storage batteries and bidirectional DC/DC buck–boost converter.

Mode One: The *S1* switch is on, and the *S2* switch is off. When power transfers from the storage units to the DC-link system during this period, the converter boosts the input voltage. This mode is activated when the stored energy must be supplied to the system.

$$\frac{di_{bat}}{dt} = \frac{V_{bat}}{L} \tag{7}$$

Mode Two: The *S1* switch is off, and the *S2* switch is on. The converter scales down the input voltage when power flows from the DC-link system to the storage units in this mode. This mode is utilized when the energy storage units require charging or replenishment.

$$\frac{di_{bat}}{dt} = \frac{V_{bat} - V_{dc}}{L} \tag{8}$$

By controlling the duty cycle of the switches, the converter efficiently modulates the voltage levels and manages the power transfer between the storage units and the DC-link system, ensuring that the stored energy is utilized most effectively.

$$\frac{di_{bat}}{dt} = \frac{V_{bat} - V_{dc}}{L} + \frac{V_{dc}}{L} \tag{9}$$

5. Battery Control

Figure 4 depicts the control of the storage battery. It involves modulating the battery current and voltage based on the SOC of both the EV and storage batteries. The upper part of the diagram illustrates the mode one operation, which occurs when the PV power is greater than 0.10 and the I_{dref} is set to zero.

The control system regulates the battery's recharge using the available PV power in this mode. The PV power is converted to 50% of the PV current as input. This value is then compared to the battery current, and a proportional-integral controller processes the result. When the I_{dref} equals zero, the PI controller generates a duty cycle that controls the storage battery's charging process during the mode one operation.

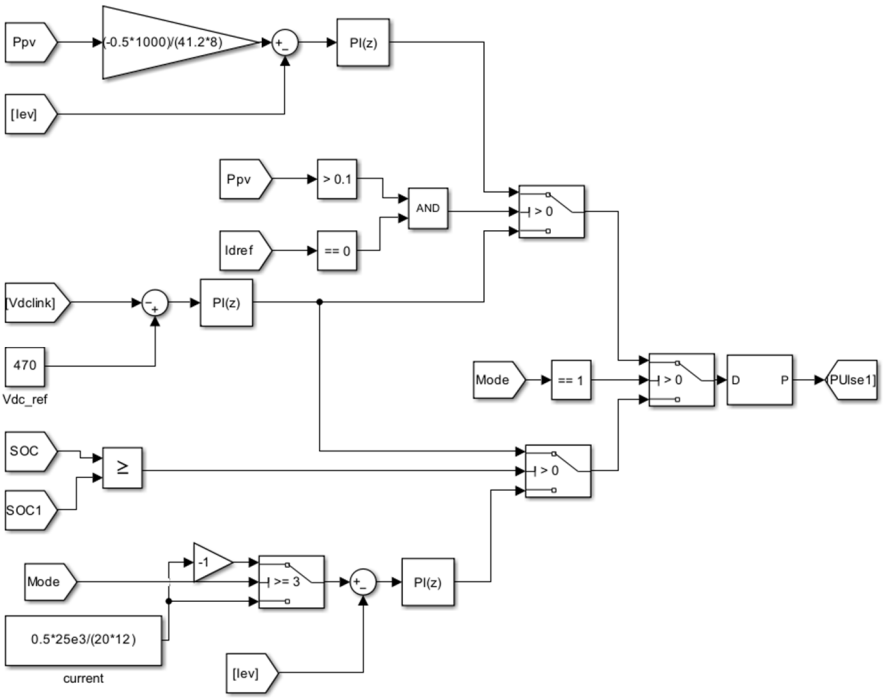

Figure 4. Battery charge and discharge controller.

Suppose the condition for mode one operation is not met, indicating that power is being sent to the grid. In that case, the control system uses a voltage control method to regulate the storage battery. This happens when the SOC of the batteries exceeds 95%.

During this operation, the control system measures and compares the DC-link voltage to the reference DC-link voltage. A PI controller is utilized to process the following voltage error. The PI controller generates a duty cycle modulated with pulse width modulation (PWM). This voltage control method ensures the storage battery is appropriately regulated when mode one operation is selected, and power is supplied to the grid.

In mode two operations, depicted in the lower portion of the figure, the control is based on the SOC of the EV and storage batteries. If the SOC is less than or equal to a specific value, denoted as SOC1 (representing the charge status of the EV battery), the control system regulates the storage battery using a voltage control process.

If this condition is not met, indicating that the SOC1 is greater than the SOC, the control switches to a current control method, as depicted in the battery unit control's lower section.

In addition, the control system verifies the mode of operation between modes two and three, previously described as V2G (vehicle-to-grid) and G2V (grid-to-vehicle) operations. The control system generates a negative current if the mode of operation is greater than or equal to three, indicating G2V operation. A PI controller then compares this negative current to the storage battery current and processes the difference. The PI controller ensures the appropriate charging process regulation and control when the grid charges the storage battery.

When the mode of operation is set to two, the control system produces a positive current, indicating that the system is operating in V2G (vehicle-to-grid) mode. This positive current is then compared to the storage battery current before being processed by a PI controller to determine the duty cycle. The duty cycle is utilized to regulate the operation of the battery in accordance with the specific mode of operation and the SOC1 and SOC values. Depending on these parameters, the control system selects either current control or voltage control to regulate the charging and discharging procedures of the battery.

6. EV Battery Control

The process for controlling EV batteries is comparable to controlling storage batteries in Figure 5. However, the SOC condition is modified to be greater than or equal to SOC1. The control concept transitions from voltage to current control mode during this condition.

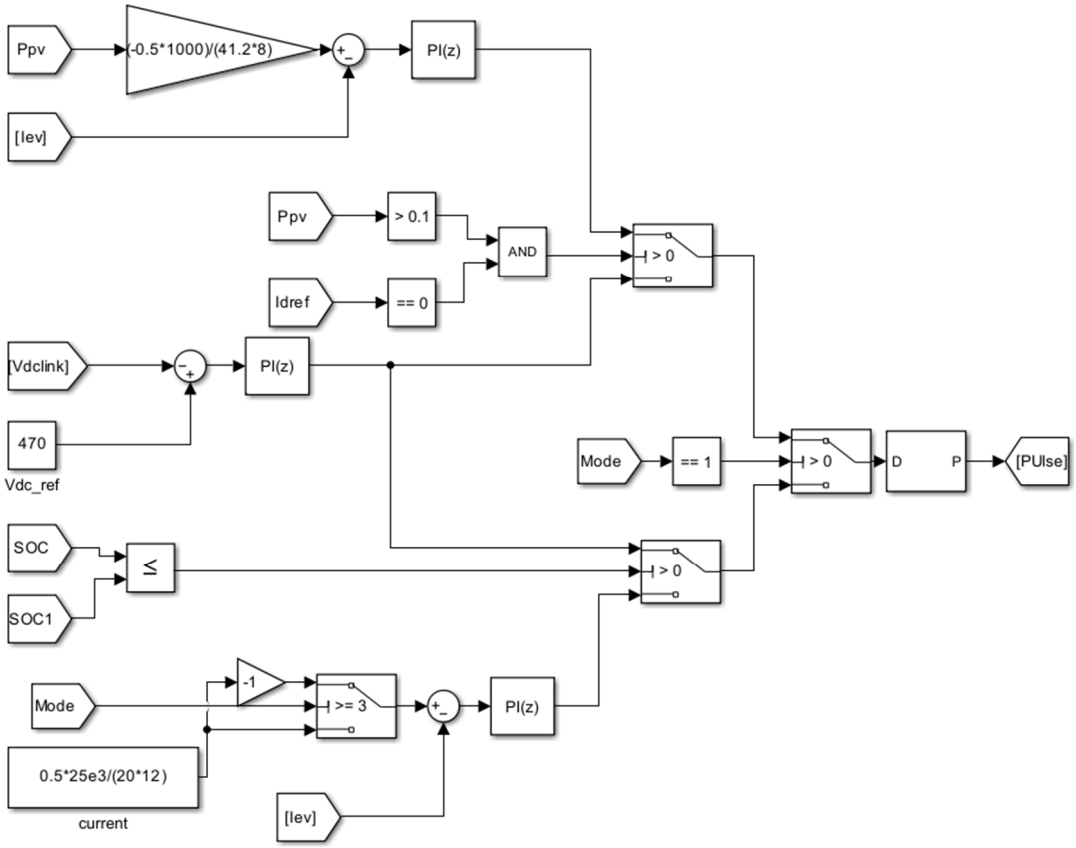

Figure 5. EVB charge and discharge controller.

The only distinction between mode two and mode three operations is the lower part of the figure, which remains the same in mode one operation. Both conditions are inverted in these modes, resulting in an inversion. Consequently, one battery is controlled using the voltage control mode, while the other is controlled using the current control mode. This enables simultaneous charging and discharging of the EV and storage battery units, facilitating effective power management operations.

7. Control of Three-Phase House Load Inverter

A unified control method is offered for an independent three-phase inverter to provide exact voltage regulation, reactive power correction, effective protection mechanisms, and frequency management as shown in Figure 6. The control method uses a closed-loop voltage control scheme to achieve perfect voltage stabilization. It monitors the output voltage and adjusts the modulation index of the inverter to maintain it at the correct level. A feedback loop that observes the reactive power at the inverter's output and adjusts the output current accordingly addresses the compensating of reactive power. This guarantees that the inverter actively manages the reactive power exchange with the load. The control method includes robust protective measures, such as protection against overvoltage and undervoltage, overcurrent protection, and short-circuit protection. These systems are designed to detect unusual conditions and respond suitably to prevent damage to both the inverter and the load. The capability to control frequency is vital in standalone systems.

As part of the control strategy's frequency control loop, the inverter's modulation index or switching frequency is modified while monitoring the output frequency to sustain the desired frequency. Techniques such as phase-locked loops (PLL) or frequency estimation methods may be used for accurate frequency management. By integrating these control objectives, the proposed method provides a comprehensive solution for standalone three-phase inverters' stable, efficient, and reliable operation. It guarantees precise voltage control, accounts for reactive power, employs strong protective measures, and keeps the output frequency constant. By using this technique, the inverter may function independently in a variety of applications without the assistance of the grid, supplying associated loads with dependable power while preserving compatibility with other parts of the power system.

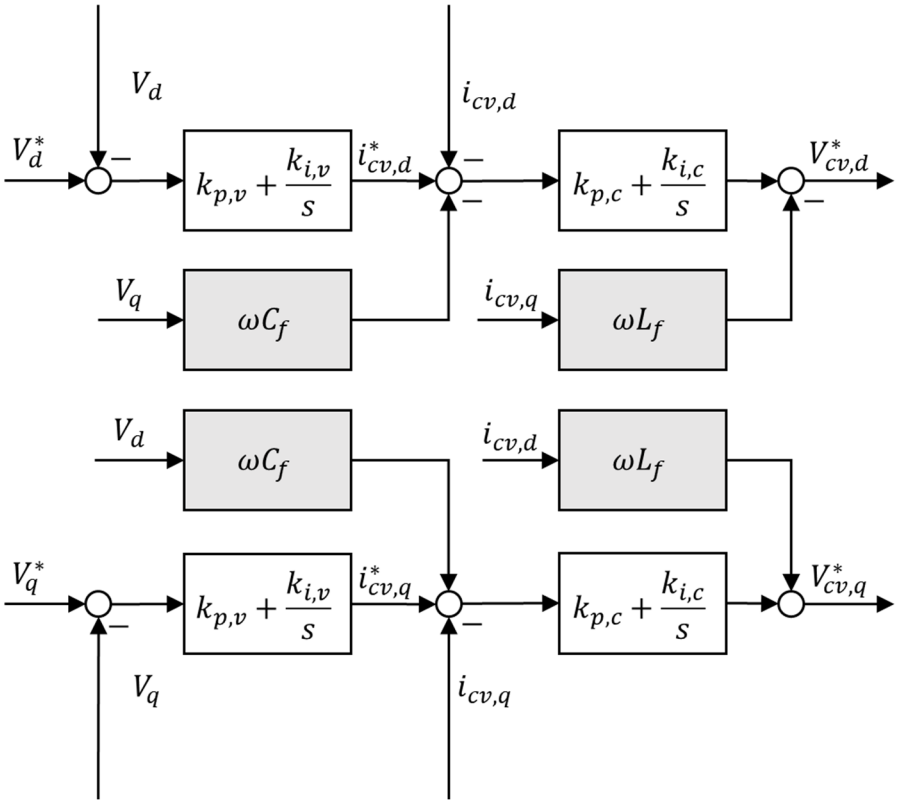

Figure 6. HLI control scheme.

8. Power Flow with Grid Forming

The LVDC-link system in Figure 7 integrates a solar panel as the primary energy source, a battery storage system, and inverters for single-phase and three-phase loads, including a grid-forming mode (GFM) inverter. The solar panel generates power ($P_{PV} = V_{PV} \cdot i_{PV}$) delivered to the DC-link through a DC/DC boost converter, while an MPPT controller ensures optimal PV performance. The battery compensates for insufficient PV power ($P_{battery} = V_b \cdot i_b$) and absorbs excess energy during surplus, maintaining DC-link stability.

The power balance at the DC-link is:

$$P_{DC-Link} = P_{PV} + P_{battery} = P_{load} \tag{10}$$

In terms of currents:

$$I_{DC} = I_{PV} + I_b \tag{11}$$

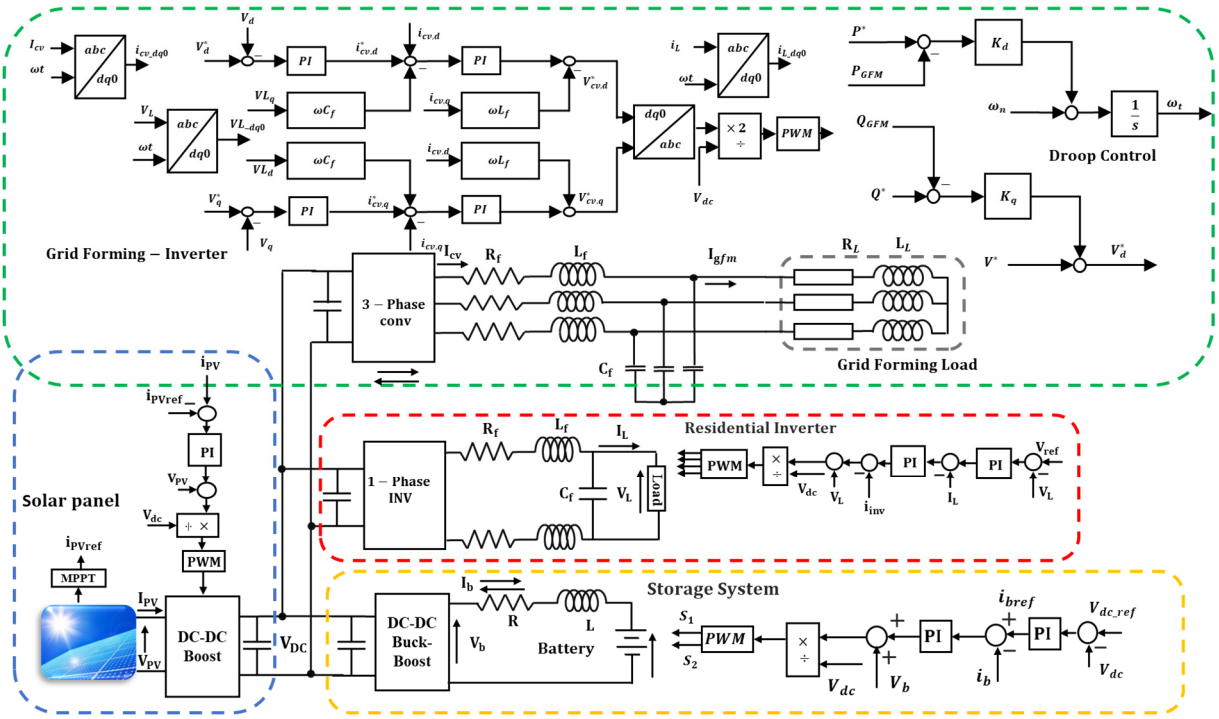

Figure 7. GFM standalone system configuration.

The system incorporates a GFM inverter designed to serve the three-phase loads. The GFM is linked to the DC-link and functions in grid-forming mode, controlling the voltage and frequency of the system. A droop control algorithm regulates power distribution between the active and reactive elements. The GFM utilizes the power available from the DC-link to feed the three-phase load, enhancing the overall stability and adaptability of the system. The total power drawn from the DC-link, including the contributions from the PV, battery, and GFM, guarantees a continuous power supply for the single-phase and three-phase loads.

The grid-forming inverter (GFM) is key in supplying power to the three-phase loads while maintaining the voltage and frequency stability. The power supplied by the GFM is given by:

$$P_{GFM} = V_{GFM} \cdot I_{GFM} \tag{12}$$

where

- V_{GFM} is the voltage at the inverter output.
- I_{GFM} is the current delivered to the load by the inverter.

The GFM dynamically adjusts its output power using droop control to ensure efficient load sharing and balance within the system. It regulates the active (P) and reactive (Q) power as follows:

$$P_{GFM} \propto \Delta\omega \text{ and } Q_{GFM} \propto \Delta V \tag{13}$$

Here, $\Delta\omega$ and ΔV represent deviations in system frequency and voltage, respectively. The GFM ensures stable operation by sharing the available DC-link power with other system components, maintaining the reliability and performance across varying load and generation conditions.

In grid-forming inverter systems, minimizing the use of analog current sensors is essential in laboratory environments where the availability of such sensors is limited. By leveraging mathematical models and known system parameters, it is possible to calculate the load current ($I_{L,dq}$) indirectly from measurable quantities like capacitor voltages and

inverter currents. This approach eliminates the need for additional sensors at the load or capacitor, making it suitable for laboratory setups with limited hardware.

At the PCC, the inverter current splits into two components:

1. The capacitor current $\left(I_{c,dq}\right)$, which is related to the dynamics of the capacitor.
2. The load current ($I_{L,dq}$), which flows to the load.

By Kirchhoff's Current Law (KCL), this relationship is expressed as follows:

$$I_{inv,dq} = I_{c,dq} + I_{L,dq} \tag{14}$$

Rearranging this gives

$$I_{L,d} = I_{inv,d} - I_{c,d} \tag{15}$$

$$I_{L,q} = I_{inv,q} - I_{c,q} \tag{16}$$

This shows that the load current is the remaining portion of the inverter current after subtracting the capacitor current.

To calculate the load current without directly measuring it, the capacitor current is first estimated using the known capacitor voltages $\left(V_{sd}, V_{sq}\right)$ and system parameters:

$$I_{c,d} = C_f \frac{dV_{sd}}{dt} + C_f \omega V_{sq} \tag{17}$$

$$I_{c,q} = C_f \frac{dV_{sq}}{dt} - C_f \omega V_{sd} \tag{18}$$

where

- C_f: Capacitance of the capacitor.
- $\frac{dV_{sd}}{dt}, \frac{dV_{sq}}{dt}$: Time derivatives of the capacitor voltages.
- ω: Angular frequency of the rotating reference frame.
- Once $I_{c,d}$ and $I_{c,q}$ are calculated, the load current can be found in Equations (17) and (18).

In this approach:

- The capacitor current is derived mathematically using the measured voltages and system parameters.
- The load current is computed without requiring a direct sensor at the load.

This method is particularly beneficial for these laboratory environments:

1. Limited Analog Sensors: The lab setup might have only a few current sensors available, and it is impractical to place sensors at every point.
2. Accuracy from Known Parameters: The method uses system parameters (e.g., capacitance C_f) and measurable voltages $\left(V_{sd}, V_{sq}\right)$ to estimate the currents accurately without additional hardware.

9. Grid-Connected Simulation Results

MATLAB/Simulink models and simulates the solar PV, storage battery, EV charging system, residential load, and grid-connected inverter based on Figure 1. Observing the system's response under various conditions allows for evaluating and validating the controllers' efficacy. Observing the system's behaviour under different conditions enables the controllers' performance to be evaluated and confirmed.

The flow diagram of Figure 8 illustrates the control procedure for the storage battery system, highlighting the decision-making steps for various operating modes depending on the power and SOC levels. Initially, the system evaluates the PV power and I_{dref}

configurations to determine the feasibility of activating mode one (PV). If mode one cannot be activated, it then reviews the SOC to choose between grid power (mode one) and alternative operational modes. When the SOC exceeds 95%, the system may persist in mode one (Grid); otherwise, it examines the possibility of mode two (V2G) or mode three (G2V) based on the predefined mode settings. This organized decision-making process guarantees that the system functions efficiently under changing power availability and storage circumstances.

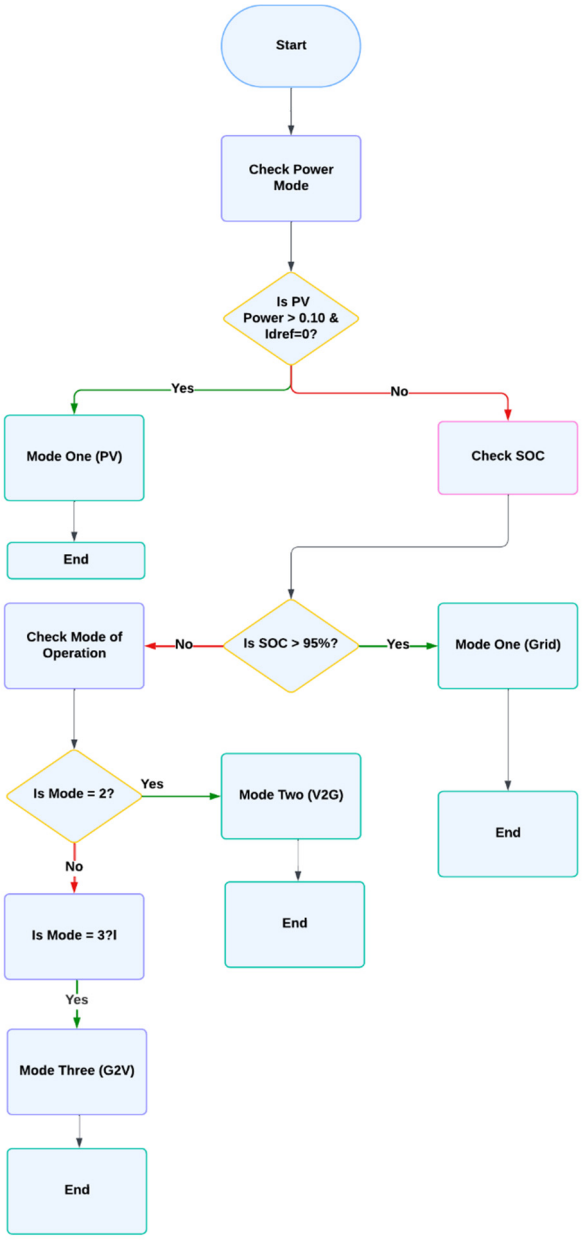

Figure 8. Mode of operations flowchart.

The simulation system parameters are listed in Table 1.

Table 1. Simulation parameters.

Parameters	Value
Grid	50 Hz, 400 V
$f_{switching}$	20 kHz
DC side	U_{dcref} = 350 V, C_{dc} = 9 × 260 µF
Power electronic unit	9 IGBTs legs
3-ph grid and GFM filter	L_s = 2.5 mH, C_s = 10 µF, R = 22 mΩ
3-ph inverter	230 V, 50 Hz
1-ph filter	L_f = 2.5 mH, C_f = 10 µF, R_{cf} = 1 mΩ R_f = 22 mΩ
	L_{dc_link} = 2 × 20 mH
1-ph load	500 W, Var as, L = 20 mH
3-ph load	5 kW, 2 kvar
Storage unit	U_{Bat} = 300 V, C_{apa} = 5000 Ah
EV battery	U_{EVBat} = 300 V, C_{apa} = 5000 Ah
PV	U_{pv} = 41.2 V, I_{max} = 10.81 A each panel
RL buck–boost inverter	L_{BDC} = 7.5 mH, R_{B_filter} = 66 mΩ
RL for PV boost inverter	L_{PVDC} = 2.5 mH, R_{PV_filter} = 22 mΩ

9.1. Mode One: Solar PV to Batteries and HLI

9.1.1. Solar PV to Batteries and HLI

Initial conditions are established by setting the irradiance to 1000 W/m^2, the temperature to 25 °C, and the initial state of charge (SOC) values for the EVB to 60% and the storage batteries to 70%.

The simulation results indicate that the PV system generates considerable energy, almost entirely eliminating the need for utility power. This result is depicted in Figure 9, which demonstrates that the PV panels charge the EV, storage batteries, and HLI, resulting in minimal grid power consumption.

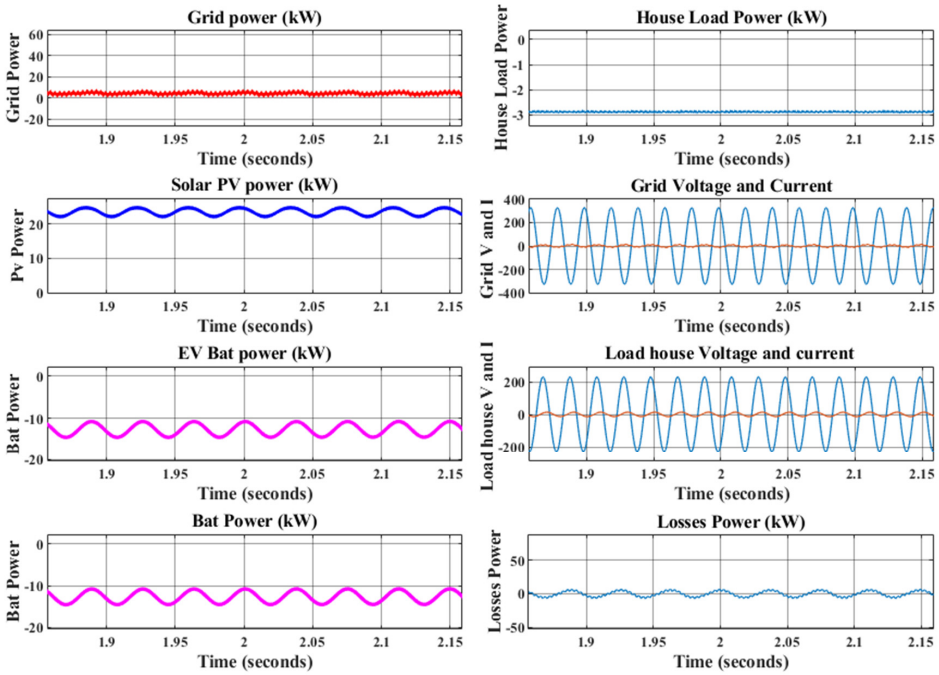

Figure 9. Mode one PV to batteries and HLI; various power values for sources and load.

Figure 10 depicts the waveforms of the grid voltage and current during mode one when the power flow is from the solar PV to the batteries and HLI. The voltage and current waveforms of the residential load on the alternating current (AC) side of the system are depicted in Figure 11.

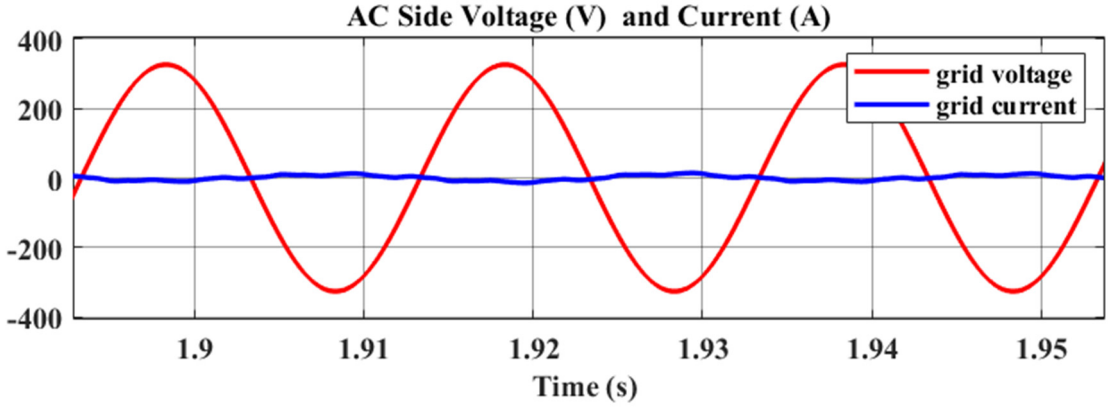

Figure 10. Mode one solar PV to batteries and HLI grid voltage and current.

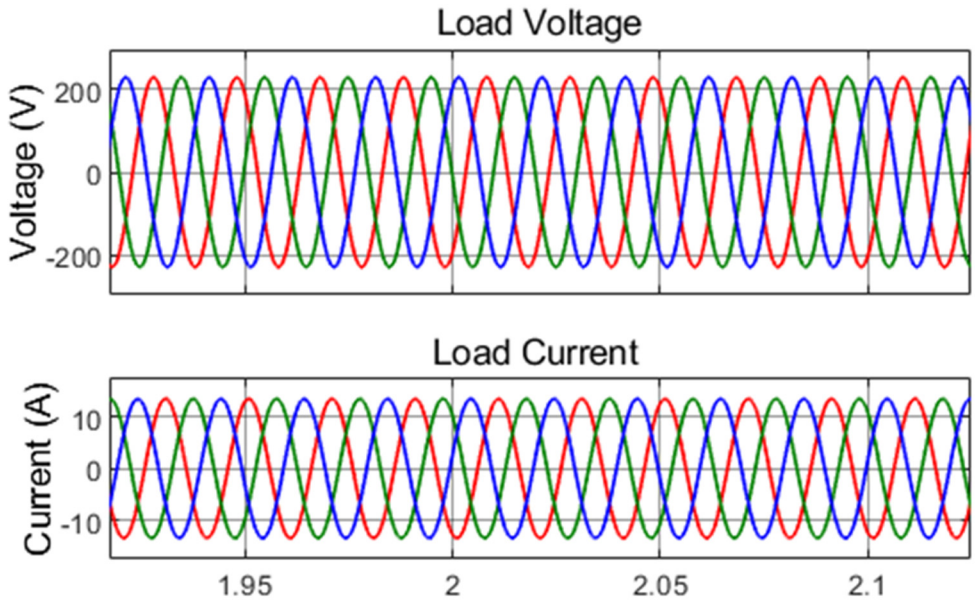

Figure 11. House load voltage and current.

9.1.2. Solar PV to Grid and HLI

Initializing the simulation parameters includes setting the irradiance to 1000 W/m^2 and the temperature to 25 °C. The EV and storage batteries also have their state of charge (SOC) set to 96%.

As depicted in Figure 12, the simulation results indicate that the power generated by the PV system is directed toward the grid and HLI. In this scenario, the power transfer to the EV and battery storage becomes negative, signifying that neither charging nor discharging is occurring. In addition, Figure 13 demonstrates that the grid current is in phase with the grid voltage, indicating that the PV system is effectively supplying the grid with the energy it generates.

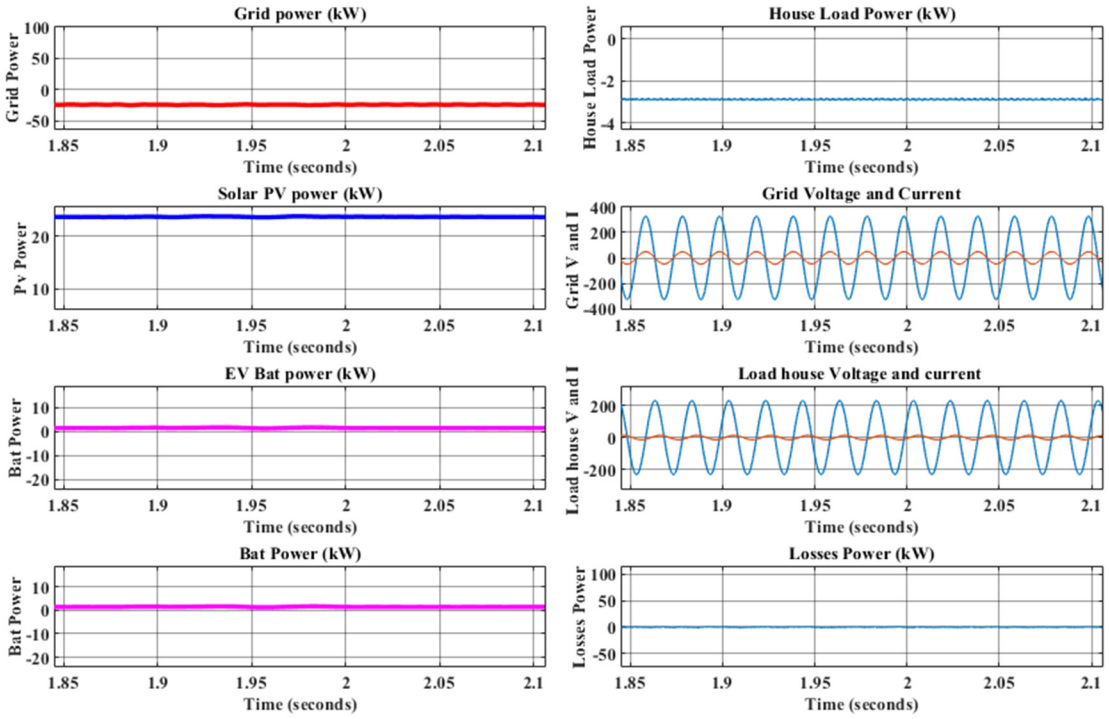

Figure 12. Mode one solar PV to grid and HLI; various power values for sources and load.

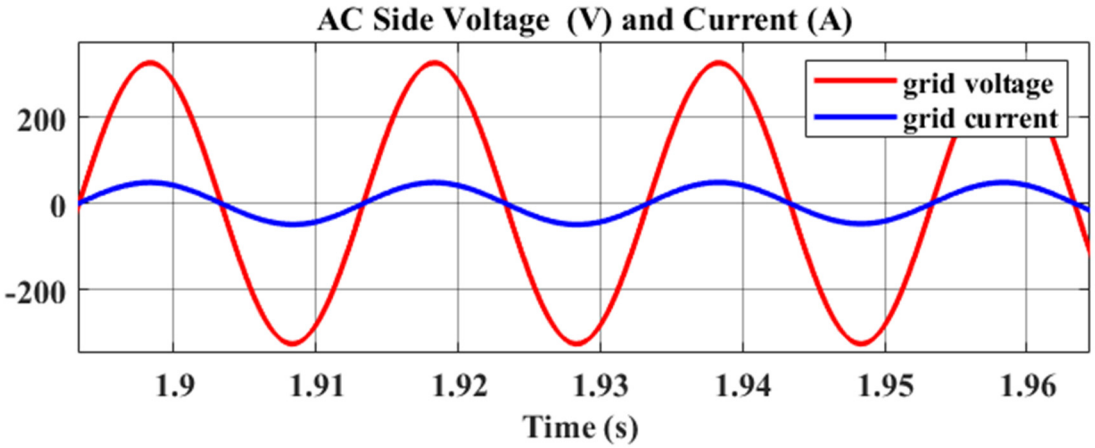

Figure 13. Grid voltage and current during mode one solar PV to grid and HLI.

9.2. Mode Two

Initializing the simulation parameters includes setting the irradiance to 0 W/m^2 and the temperature to 0 °C. In addition, the state of charge of the EV and storage batteries (SOC) are set at 60% and 70%, respectively. In addition, mode three is replaced by mode two, signifying a transition toward V2G (vehicle-to-grid) operation.

Figure 14 demonstrates that no power is extracted from the storage battery and that the PV power is negative. Due to SOC1 being lower than SOC, the EV battery charges while the storage battery discharges during mode two operation. It also demonstrates that the grid current remains in phase with the grid voltage, indicating that it receives power. In mode two, without PV power, the storage battery provides energy to the grid, HLI, and EVB charging.

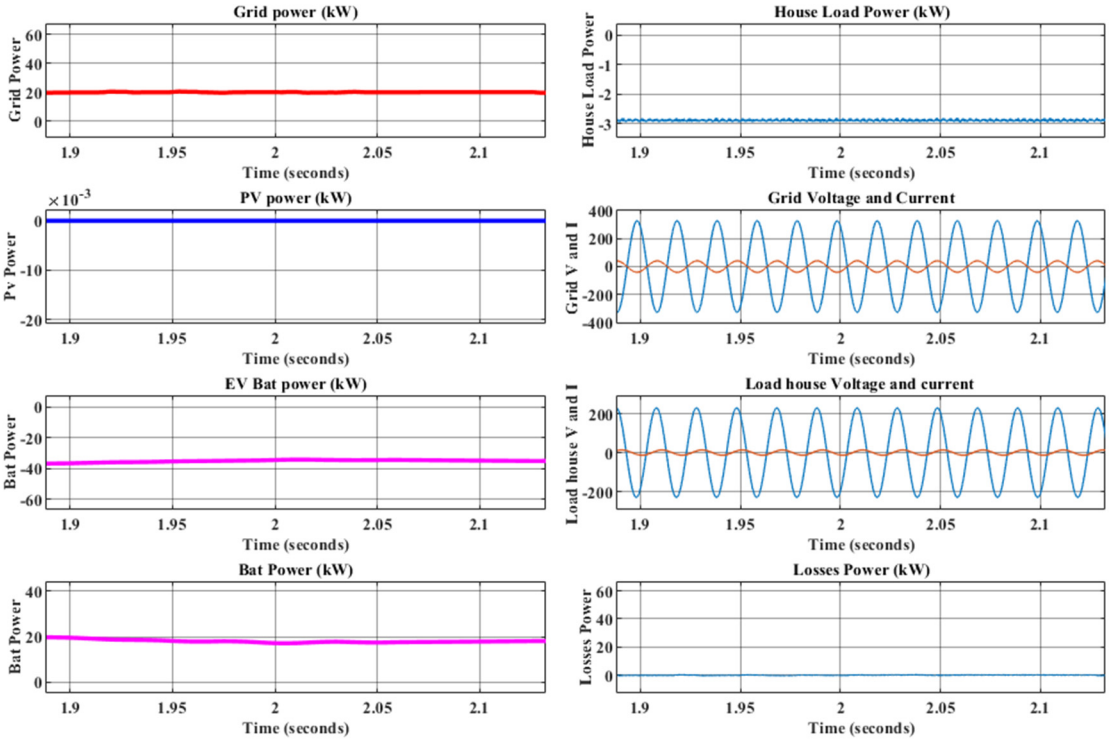

Figure 14. Various power values for sources and load during mode two.

In another operation in mode two, when the SOC1 of the EV battery is higher than the SOC of the storage battery, the previous process of mode two will be different. This means the EV battery supplies power to the storage battery charging, the HLI, and the grid without PV power in mode two. Also, the grid current is in phase with the grid voltage, which means the power is supplied to the grid, as shown in Figure 15.

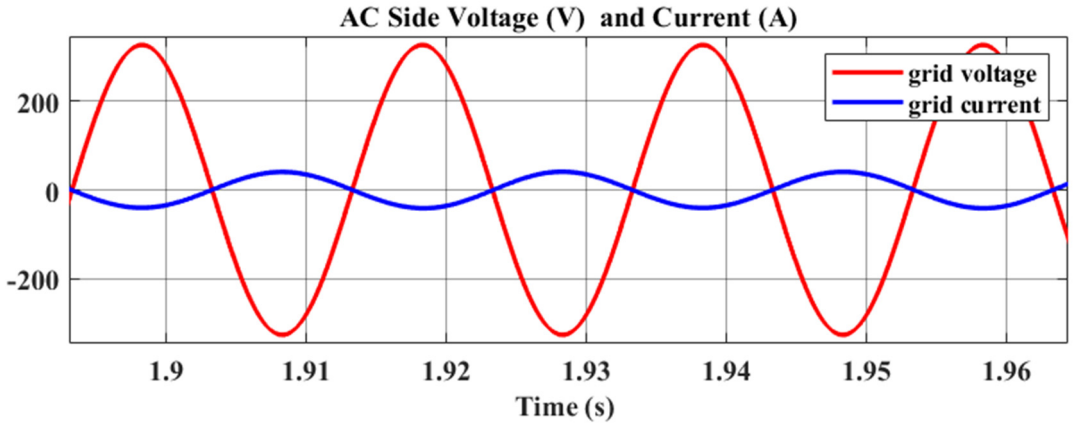

Figure 15. Grid voltage and current during mode two and three.

9.3. Mode Three

The simulation begins by initializing the parameters, with the irradiance and temperature set to 0 W/m^2 and 0 °C, respectively. The state of charge is set to 60% for the EV and 70% for the storage batteries. In addition, the mode selection is changed from two to three, signifying a transition to grid-to-vehicle (G2V) operation.

The results depicted in Figure 16 indicate no power loss from the PV source. During mode three, the EV battery charges from the utility during the storage battery discharges because SOC1 is less than SOC. In addition, Figure 15 demonstrates that the grid current is out of phase with the grid voltage, indicating that the system draws power from the

grid. In mode three, the EV charging and HLI operations are powered by grid power and storage batteries in the absence of PV power.

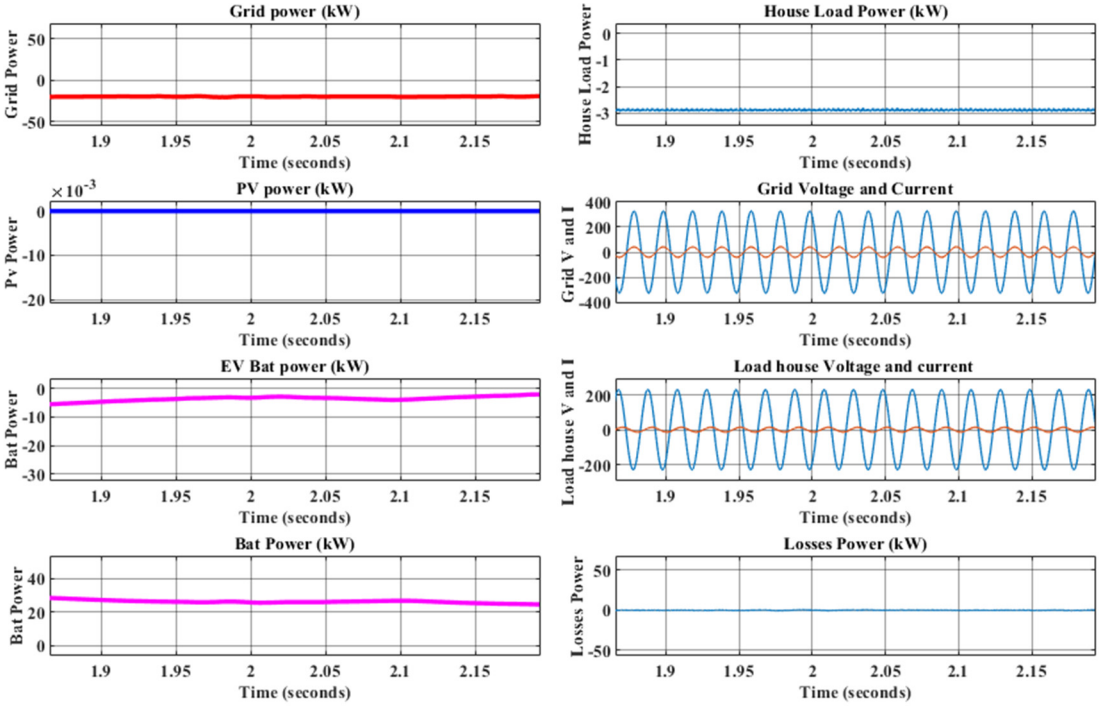

Figure 16. Various power values during mode two when SOC1 is higher than SOC.

In another mode (Figure 17), in three scenarios, the SOC1 of the EV battery is greater than that of the storage battery. This variation in the mode three operations leads to a distinct power transfer configuration; specifically, the storage battery charges from utility power, whereas the EV battery discharges because SOC1 is less than SOC. Similarly, Figure 15 demonstrates that the grid current is not synchronized with the grid voltage, indicating that the system draws power from the grid. In mode three, without PV power, the EV charging and HLI operations are powered by both the grid and the storage battery.

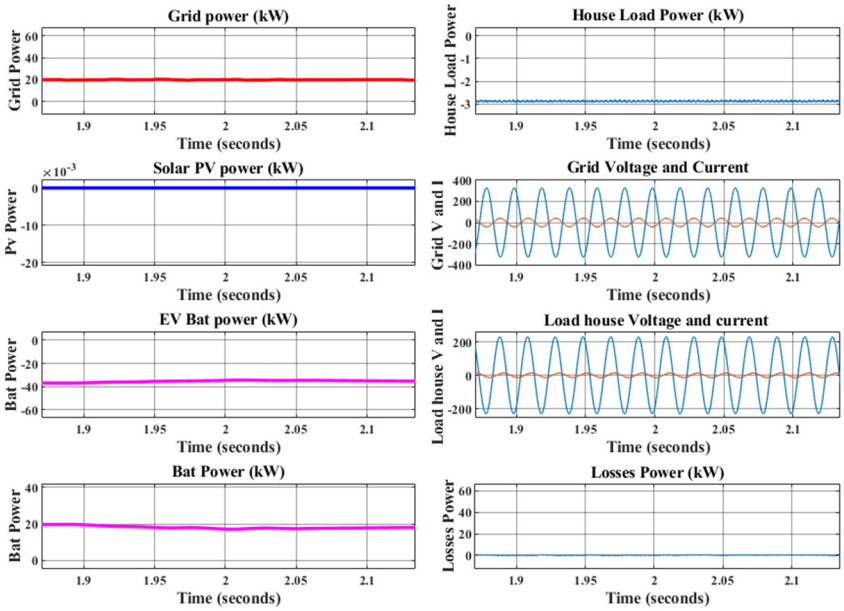

Figure 17. Various power values for sources and load during mode three.

10. Laboratory Implementation of GFM Case Study

In laboratory environments with limited analog current sensors, the load current ($I_{L,dq}$) in grid-forming inverters can be calculated using measured capacitor voltages and known system parameters. By estimating the capacitor current $\left(I_{c,dq}\right)$ and subtracting it from the inverter current ($I_{inv,dq}$), the load current can be determined without requiring additional sensors.

Figure 18 depicts an Imperix control model created for a microgrid system. It incorporates various control layers to regulate energy flow and maintain stability across grid-forming, load management, and renewable energy integration. The grid-forming component utilizes droop control techniques to balance active and reactive power alongside cascaded voltage and current control loops for accurate regulation. The House Load Inverter guarantees power delivery to the connected loads, while the Battery Converter Control and PV Converter Control oversee energy storage and photovoltaic inputs, respectively.

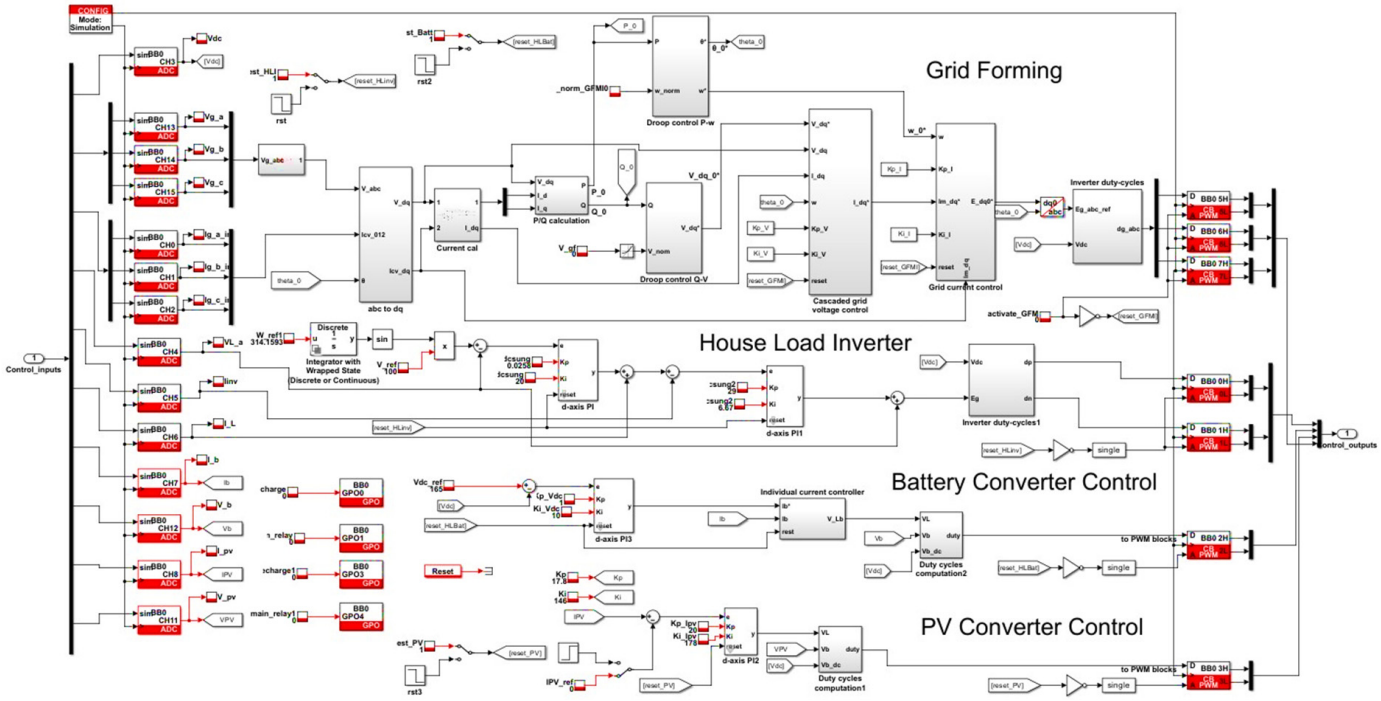

Figure 18. Imperix system configuration.

The laboratory configuration includes Imperix power modules, a residential inverter, and an energy storage system, as shown in Figure 19. The Imperix modules control the energy flow through three-leg and two-leg configurations with built-in measurement capabilities. The residential inverter provides AC power to loads and evaluates grid-forming functionalities. The storage system combines batteries with precharging mechanisms for energy swapping. This modular arrangement enables accurate monitoring and validation of the proposed LVDC B2B converter system in real-world scenarios.

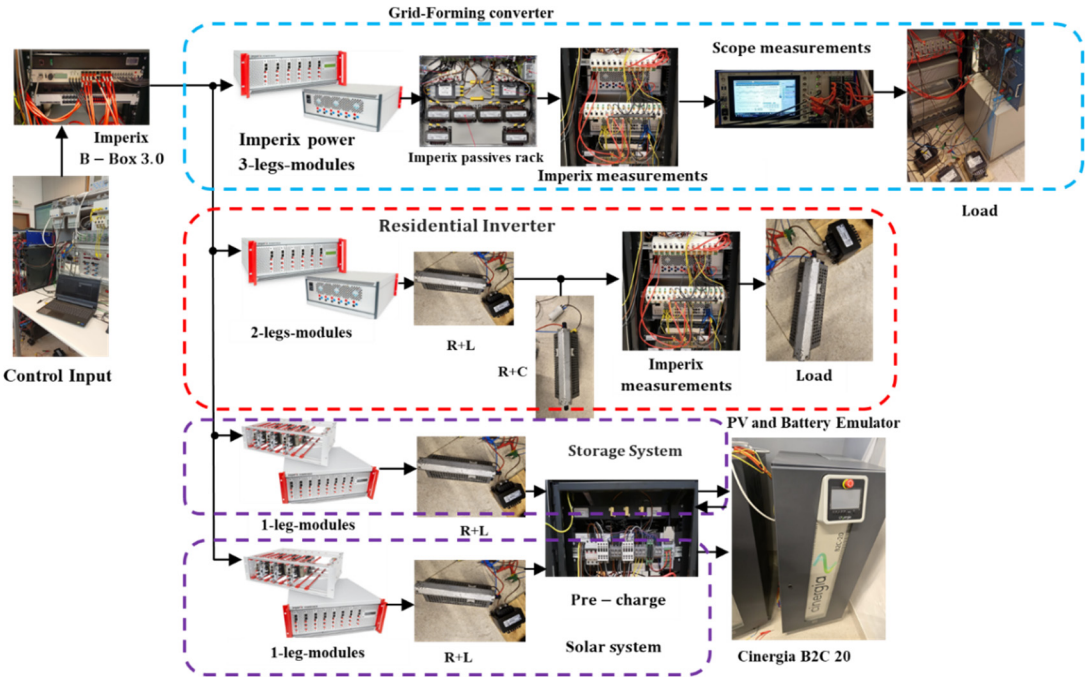

Figure 19. System configuration.

Table 2 shows the experimental system parameters.

Table 2. Experimental system parameters.

Parameters	Value
$f_{switching}$	20 kHz
DC side	U_{dcref} = 200 V, C_{dc} = 7 × 260 µF
Power electronic unit	7 IGBTs legs
3-ph filter GFM	L_s = 2.5 mH, C_s = 10 µF, R = 22 mΩ
3-ph GFM inverter	L.L rms 100 V, 50 Hz
1-ph inverter	100 V, 50 Hz
1-ph filter	L_f = 2.5 mH, C_f = 10 µF, R_{cf} = 1 mΩ, R_f = 22 mΩ
	L_{dc_link} = 2 × 20 mH
1-ph load	500 W, Var as, L = 20 mH
3-ph load GFM	1000 W, Var as L = 20 mH
Storage emulator	U_{Bat} = 162 V, C_{apa} = 20 Ah
PV emulator	U_{pv} = 30 V, I_{max} = 5 A each panel
RL buck–boost inverter	L_{BDC} = 7.5 mH, R_{B_filter} = 66 mΩ
RL for PV boost inverter	L_{PVDC} = 2.5 mH, R_{PV_filter} = 22 mΩ

10.1. Modes of Operation

The LVDC system dynamically transitions between operating modes based on solar energy availability and load demand.

In low or insufficient irradiance, the battery discharges via the buck–boost converter to sustain the DC-link voltage and provide power to the load. Figure 20 illustrates the system that activates the battery buck–boost converter, maintaining a dc-link voltage reference equal to the battery voltage. Subsequently, we gradually increase the $Vdc_{\_ref}$ until we reach

the target value of 200 V. During this process, it is observed that both the HLI and PV currents are at zero. In contrast, the battery current remains minimal for the dc-link voltage.

Figure 20. Only battery connected feeding to the dc-link.

10.2. Battery Charge

When the photovoltaic array produces more power than the load needs, surplus energy is utilized to recharge the battery. The battery storage captures the excess current, which helps to avoid overvoltage in the DC-link, as illustrated in Figure 21.

Figure 21. Excess energy is used to charge the battery.

10.3. Both PV and Battery Charge

Figure 22 illustrates the operation of the LVDC system with the PV array, battery, and GFM under varying conditions. The top section shows the DC-link, PV, and battery voltage, indicating stable operation at their respective levels. The waveforms of the three-phase GFM output voltages and currents highlight balanced sinusoidal operation. The PV and battery currents demonstrate dynamic load sharing, with the PV providing the primary support while the battery compensates for the deficit. The bottom graphs display the power

flows at different points in the system, confirming efficient energy management and stable load supply.

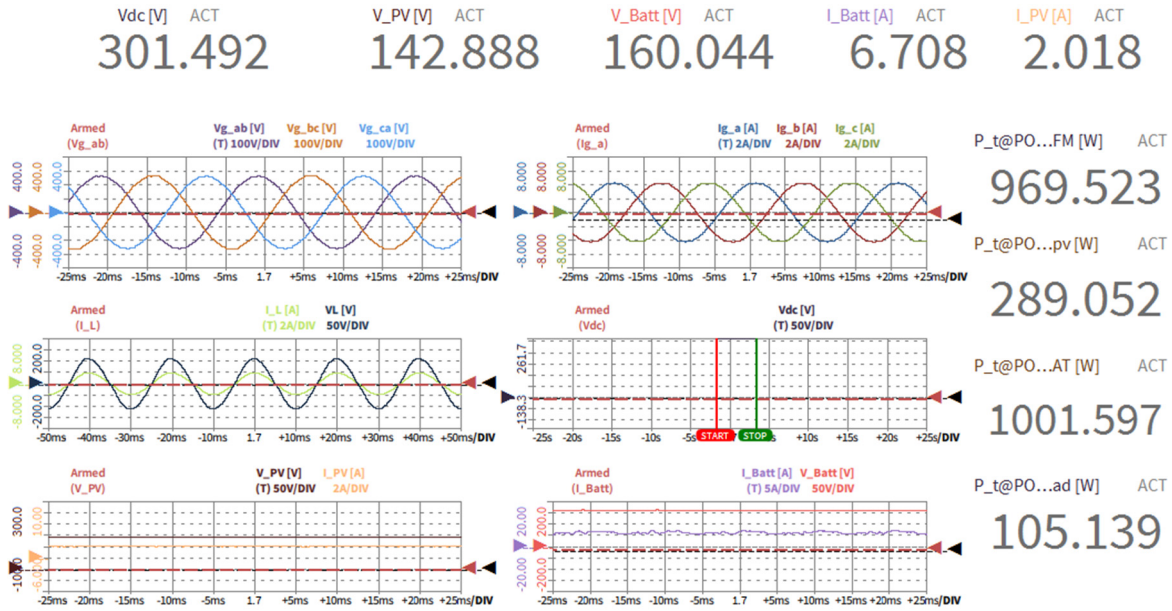

Figure 22. Battery and PV feeding into dc-link.

10.4. GFM Load Changes

Figures 23 and 24 depict the system's performance under load imbalance conditions in the GFM, as shown in the GFM current waveforms at the top right. Despite the unbalanced load, the system remains stable across all components, including the DC-link voltage, PV output, and battery functionality. The consistent sinusoidal output voltage of the GFM illustrates the system's resilience, ensuring dependable operation and load distribution even under challenging situations. This emphasizes the effectiveness of the control strategies in sustaining system performance.

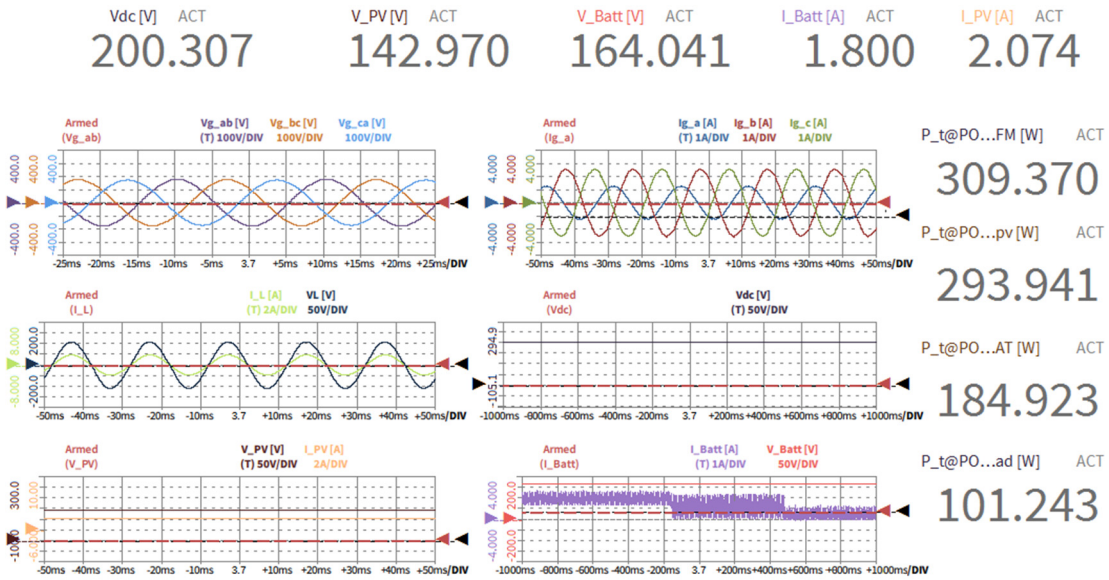

Figure 23. Unbalanced GFM load.

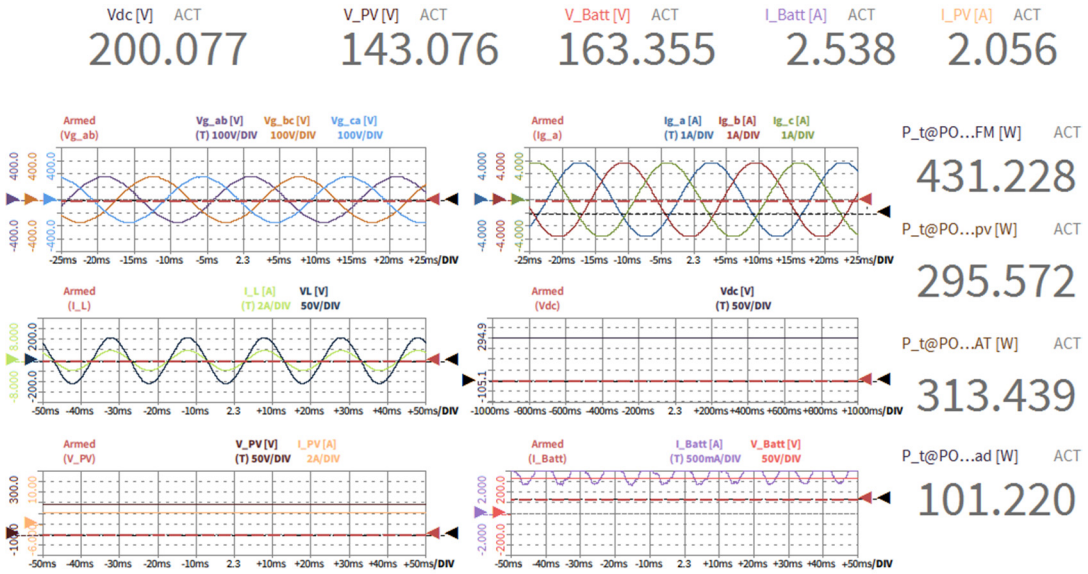

Figure 24. Balanced GFM with increased load.

Figure 25 shows the system's capability to adapt to an elevated DC-link voltage (VDC) of 300 V, which is necessary to match the increased output voltage of the grid-forming inverter (GFM). This modification allows the GFM to sustain consistent three-phase output voltages while fulfilling the needs of the connected loads. Raising the DC-link voltage stabilizes the power flow from the PV and battery systems to the GFM, ensuring all components function harmoniously. The waveforms demonstrate that the system remains strong and stable, facilitating a smooth transition amidst changing voltage conditions.

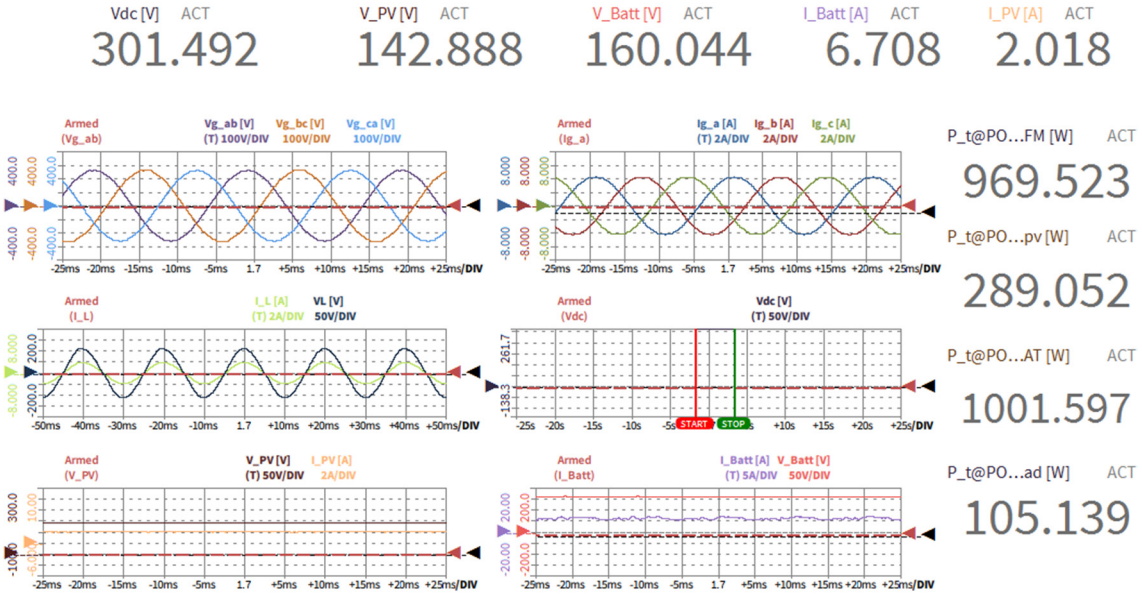

Figure 25. Increasing GFM voltage and DC-link voltage.

Throughout the entire operation, the system's performance was closely observed in Figure 26, particularly focusing on the functioning of the PV and battery. The green line indicates the PV system's voltage, current, and power, while the red line reflects the input from the battery. The graphs depict the dynamic interplay between the PV and battery systems:

- The PV system mainly powers the load, modifying its output in response to the solar availability.

- The battery system offsets any deficits from the PV by discharging when there is a need for extra power and charging when there is surplus energy, thus ensuring stable DC-link operations.

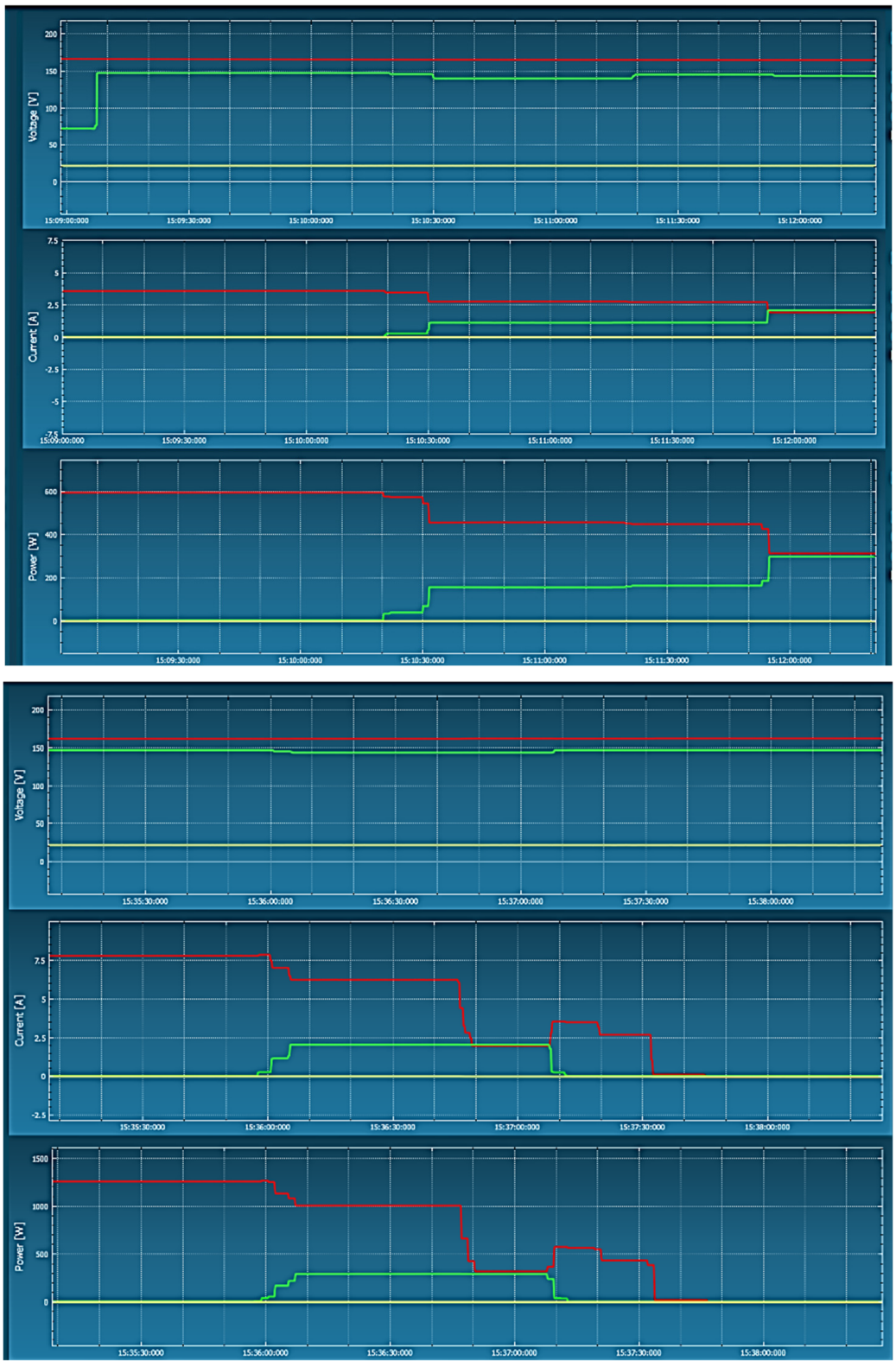

Figure 26. Cinergia battery and PV emulator monitor.

This collaborative interaction showcases the system's capability to effectively balance renewable energy sources with battery storage, sustaining reliability under different circumstances.

11. Conclusions

This study developed and verified an LVDC B2B converter system that integrates PV panels, EVs, storage batteries, and a grid-connected inverter via a common DC-link. The system showed effective energy exchange, stable performance in both grid-connected and microgrid modes, and smooth transitions between different operational states. A significant innovation is the implementation of sensorless current estimation in the grid-forming inverter, which reduces the hardware requirements while ensuring precision. Both simulations and experimental tests validated the high utilization of PV, dependable EV charging, and efficient power flow management. This research offers a scalable approach for incorporating renewable energy and storage into low-voltage networks, setting the stage for future developments in predictive energy management and real-time system validation.

The main contributions of this study include the following:

- Bidirectional LVDC B2B Converter and Hybrid Control Strategy: Designed to improve energy transfer and isolation in low-voltage networks, ensuring voltage stability and adaptive power management under varying conditions.
- Sensorless Current Estimation and Experimental Validation: A method to eliminate the need for analog sensors while maintaining accurate current measurement, validated through simulations and laboratory tests, leading to efficient power management.

12. Future Work

Future efforts will focus on enhancing sensorless current estimation methods to better their reliability under diverse conditions and expand the system's scalability for wider applications. Progress in strong predictive algorithms and thorough real-time validation methods will be essential in tackling these issues, setting the foundation for more robust and flexible energy systems in low-voltage networks.

Author Contributions: Conceptualization, Z.H.A. and D.R.; Methodology, Z.H.A. and D.R.; Software, Z.H.A. and D.R.; Validation, Z.H.A. and D.R.; Formal analysis, Z.H.A. and D.R.; Investigation, Z.H.A. and D.R.; Resources, Z.H.A. and D.R.; Data curation, Z.H.A. and D.R.; Writing—original draft, Z.H.A.; Writing—review & editing, D.R.; Visualization, Z.H.A. and D.R.; Supervision, D.R.; Project administration, D.R.; Funding acquisition, D.R. All authors have read and agreed to the published version of the manuscript.

Funding: The research was financed in part by the project no. FIEK_16-1-2016-0007 has been implemented with the support provided by the National Research, Development, and Innovation Fund of Hungary, financed under the FIEK_16 funding scheme.

Data Availability Statement: The original contributions presented in this study are included in the article. Further inquiries can be directed to the corresponding author.

Acknowledgments: The authors thank the BME Smart Power Laboratory (SPL) for supporting this research.

Conflicts of Interest: The authors declare no conflict of interest.

References

1. Vinayagam, A.; Swarna, K.S.V.; Khoo, S.Y.; Oo, A.T.; Stojcevski, A. PV Based Microgrid with Grid-Support Grid-Forming Inverter Control-(Simulation and Analysis). *Smart Grid Renew. Energy* **2017**, *8*, 1–30. [CrossRef]

2. Chauhan, S.; Singh, B. Grid-interfaced solar PV powered electric vehicle battery system with novel adaptive digital control algorithm. *IET Power Electron.* **2019**, *12*, 3470–3478. [CrossRef]
3. Arfeen, Z.A.; Khairuddin, A.B.; Larik, R.M.; Saeed, M.S. Control of distributed generation systems for microgrid applications: A technological review. *Int. Trans. Electr. Energy Syst.* **2019**, *29*, e12072. [CrossRef]
4. Biya, T.S.; Sindhu, M.R. Design and Power Management of Solar Powered Electric Vehicle Charging Station with Energy Storage System. In Proceedings of the 2019 3rd International Conference on Electronics, Communication and Aerospace Technology (ICECA), Coimbatore, India, 12–14 June 2019; pp. 815–820. [CrossRef]
5. Dehaghani, M.N.; Abbas Taher, S.; Arani, Z.D. Coordinated control of hybrid AC/DC microgrids including PV and storage systems. *Energy Equip. Syst.* **2021**, *9*, 307–316.
6. Ahmadi, M.; Kaleybar, H.J.; Brenna, M.; Castelli-Dezza, F.; Carmeli, M.S. Implementation of DC Micro Grid Tied PV-Storage Based EV Fast Charging Station. In Proceedings of the 2021 IEEE International Conference on Environment and Electrical Engineering and 2021 IEEE Industrial and Commercial Power Systems Europe (EEEIC/I&CPS Europe), Bari, Italy, 7–10 September 2021. [CrossRef]
7. Ahmadi, M.; Jafari Kaleybar, H.; Brenna, M.; Castelli-Dezza, F.; Carmeli, M.S. Integration of Distributed Energy Resources and EV Fast-Charging Infrastructure in High-Speed Railway Systems. *Electronics* **2021**, *10*, 2555. [CrossRef]
8. Gupta, S.; Verma, A.; Singh, B.; Garg, R.; Singh, A. IZAQ-LMS-based control of PV-battery interfaced microgrid in grid-connected and autonomous modes. *IET Power Electron.* **2020**, *13*, 3999–4007. [CrossRef]
9. Savio Abraham, D.; Verma, R.; Kanagaraj, L.; Giri Thulasi Raman, S.R.; Rajamanickam, N.; Chokkalingam, B.; Marimuthu Sekar, K.; Mihet-Popa, L. Electric vehicles charging stations' architectures, criteria, power converters, and control strategies in microgrids. *Electronics* **2021**, *10*, 1895. [CrossRef]
10. Wang, Y.; Ren, B.; Liyanage, S. Unified control scheme for a dual-stage grid-connected PV system with mode change. *Sol. Energy* **2022**, *239*, 88–101. [CrossRef]
11. Ali, Z.H.; Saleh, Z.H.; Daoud, R.W.; Ahmed, A.H. Design and simulation of a microgrid for TIH campus. *Indones. J. Electr. Eng. Comput. Sci.* **2020**, *19*, 729–736. [CrossRef]
12. Panda, S.S.; Rout, U.K. Control and Management of Power Exchange in Microgrid. In Proceedings of the 2022 IEEE 2nd International Symposium on Sustainable Energy, Signal Processing and Cyber Security (iSSSC), Gunupur, Odisha, India, 15–17 December 2022; pp. 1–6. [CrossRef]
13. Buts, K.; Dewan, L.; Prasad, M.P.R. PI-Based Feedback Control Technique for Current Control of the Battery Energy Storage System. In Proceedings of the 2022 IEEE 10th Power India International Conference (PIICON), New Delhi, India, 25–27 November 2022. [CrossRef]
14. Nanda, A.A.; Narayanan, V.; Singh, B. Control of a Central Battery Energy Storage System and Solar PV Based Microgrid in GI and SA Modes. In Proceedings of the 2022 IEEE 10th Power India International Conference (PIICON), New Delhi, India, 25–27 November 2022. [CrossRef]
15. Khemissi, L.; Khalfa, M.-A.; Sellami, A. Control and Energy Management of Wind/PV/Battery Smart Microgrid. In Proceedings of the 2022 IEEE International Conference on Electrical Sciences and Technologies in Maghreb (CISTEM), Tunis, Tunisia, 26–28 October 2022. [CrossRef]
16. Gupta, M.; Seth, A.K.; Singh, M. Grid Tied Photovoltaic Based Electric Vehicle Charging Infrastructure. In Proceedings of the 2022 Second International Conference on Advances in Electrical, Computing, Communication and Sustainable Technologies (ICAECT), Bhilai, India, 21–22 April 2022. [CrossRef]
17. Seth, A.K.; Singh, M. Plant integrated proportional integrating based control design for electric vehicle charger. *Comput. Electr. Eng.* **2023**, *105*, 108522. [CrossRef]
18. Makhanya, T.; Sewsunker, R.; Pillay, N. A Distributed Standalone Solar PV and Battery Energy Storage System DC Microgrid. In Proceedings of the 2023 31st Southern African Universities Power Engineering Conference (SAUPEC), Johannesburg, South Africa, 24–26 January 2023; pp. 1–6. [CrossRef]
19. Bhattar, C.L.; Chaudhari, M.A. Centralized Energy Management Scheme for Grid Connected DC Microgrid. *IEEE Syst. J.* **2023**, *17*, 3741–3751. [CrossRef]
20. Jain, V.; Singh, B. Seema A Grid Connected PV Array and Battery Energy Storage Interfaced EV Charging Station. *IEEE Trans. Transp. Electrif.* **2023**, *9*, 3723–3730. [CrossRef]
21. Abd El Baset Abd El Halim, A.; Hassan Eid Bayoumi, E.; El-Khattam, W.; Mohamed Ibrahim, A. An improved equalization technique for fast charging of Electric vehicles. *Ain Shams Eng. J.* **2024**, *15*, 102727. [CrossRef]
22. Ali, Z.H.; Raisz, D. Experimental validation of a Low-Voltage Back-to-Back Converter Control Strategy. In Proceedings of the 2024 6th Global Power, Energy and Communication Conference (GPECOM), Budapest, Hungary, 4–7 June 2024; pp. 103–108. [CrossRef]

23. Hassen, W.F.; Schoppik, L.; Schiegg, S.; Gerl, A. Power Management Approach of Hybrid Energy Storage System for Electric Vehicle Charging Stations. *Smart Cities* **2024**, *7*, 4025–4051. [CrossRef]
24. Xing, Y.; Qin, W.; Zhu, H.; Liu, K.; Zhou, C. Research on Energy Management Technology of Photovoltaic-FESS-EV Load Microgrid System. *World Electr. Veh. J.* **2024**, *15*, 508. [CrossRef]